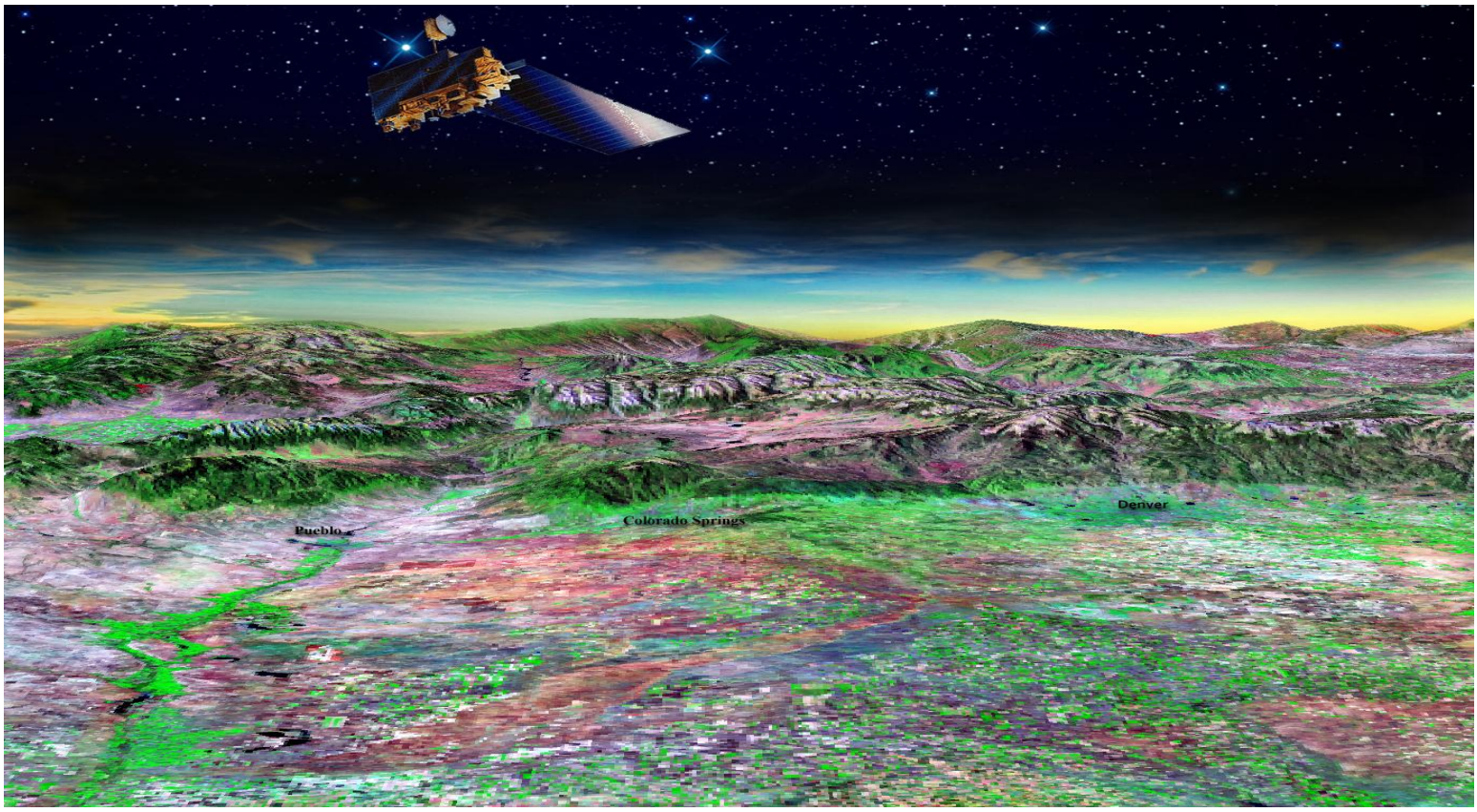

Identifying and Delineating Thermally Active Areas in Colorado Using Thermal Remote Sensing Data

Final Report
Department of Energy (DOE) Project
DOE Grant DE-EE0002828
12/26/2012

Submitted to
Flint Geothermal LLC, Denver, Colorado

By
Khalid A. Hussein

Earth Science & Observation Center (ESOC)
Cooperative Institute for Research in Environmental Sciences (CIRES)
University of Colorado, Boulder

Table of Contents

List of Figures

1. Introduction and Background

The United States has immense amount of heat stored underground whose full potential has yet to be realized, and this geothermal energy flows continuously to the surface. The recovery of even a very small percentage of this heat would make a large difference to the nation's energy supplies (Green and Nix, 2006). The State of Colorado has a high potential of geothermal energy remaining to be discovered and recovered. Thermally active areas are known to exist throughout the state of Colorado and the western U.S. These areas can serve as a potential source of significant geothermal energy for electrical power generation. However, drilling to find these sources is a costly and logistically complex activity, which can sometimes inhibit the exploitation of this important natural energy source. As a result, there is considerable value in being able to systematically identify these thermally active regions with high spatial resolution remote sensing over large areas. Identifying the areas showing the greatest promise will reduce the risk of drilling and increase the likelihood of successfully identifying commercial resources. Satellite remote sensing provides an excellent opportunity to identify thermally active areas that have a high potential for commercial applications. Currently, the main techniques for identifying possible sources of geothermal heat rely on ground-based measurements, which are inefficient and very local in nature.

Remote sensing data acquired by thermal sensors onboard different platforms have been used to locate areas of geothermal activity (Coolbaugh et al., 2007; Eneva et al., 2007; 2006; Eneva and Coolbaugh, 2009; Vaughan et al., 2012). Historically, the principal reason for thermal infrared (TIR) measurements has been to estimate temperatures from thermal infrared radiances which vary with both temperature and emissivity (Gillespie et al., 1998). Since the emissivity of water is well defined, the TIR remote sensing data is used to measure and monitor sea surface temperature (Anding and Kauth, 1970; Barton, 1985; Kilpatrick et al., 2001; McConaghy, 1980; McMillin and Crosby, 1984; Noble and Wilkerson, 1970; Prabhakara et al., 1974; Walton, 1985). Large errors occur if the same techniques applied to retrieve sea surface temperature are used for the recovery of land surface temperature, because the emissivity of the surface is unknown. Therefore, studies require accurate land surface temperature limited to those cases where the surface emissivity is known (Kealy and Hook, 1993). Various techniques that separate temperature and emissivity in the multispectral thermal infrared such as the reference channel, the emissivity normalization, and the alpha derived emissivity have been developed. These

techniques differ based on the assumptions they make. The reference channel method assumes a constant emissivity value for a certain channel. The emissivity normalization method resembles the reference channel, except the constant emissivity value is used for each channel and the highest temperature is assigned to the pixel. The alpha derived emissivity is based on Wien's approximation of the Plank function (Gillespie et al., 1998; Hook et al., 1992; Kealy and Hook, 1993, Tang et al., 2004; 2007HH).

Land surface temperature of geothermally active areas is composed of two components: (1) temperature due to solar radiation absorbed by the surface (which is influenced by elevation as well as surface orientation - slope and aspect), and (2) temperature as a result of geothermal heat. It is difficult to separate between the temperature anomalies due to solar radiation with topographic effects and anomalies due to geothermal heat. Recently, numerous studies have suggested some techniques and methods to compensate for solar and topographic effects. For example, Coolbaugh et al. (2007) mapped surface temperature anomalies associated with geothermal activity at Bradys Hot Springs, Nevada, USA, by processing the Advanced Spaceborne Thermal Emission Reflection Radiometer (ASTER) thermal data to minimize the albedo, slope and diurnal heat effects. The albedo was corrected using the visible and near infrared bands of ASTER, slope was corrected using digital elevation model (DEM). The diurnal heat effects were corrected using 24 hours surface temperature measurements in integration with ASTER day and night time data. A simple energy balance assuming the latent heat flux is negligible was used. Their method is suited for dry or desert areas like Nevada; however it is difficult to apply such a method in moist and vegetated areas. Moreover, the method needs a pair of day and nighttime data, for the same day and it is not easy to find such pair in the Earth Resources Observation Systems (EROS) Data Center, and in particular, for large areas. An alternative to the forgoing there are spatial-based models that compute the spatial and temporal variations of the incoming solar radiation (insolation).

Spatial insolation models can be categorized into two types: point specific and area based (Fu and Rich, 1999). Point specific models calculate insolation for a location, while area based calculate insolation for a geographic area. Fu and Rich (1999) developed the Solar Analyst, a geometric solar radiation model that calculates the amount of the incoming solar radiation and can be utilized in different fields including, forestry, civil engineering, agriculture, ecology, and environmental assessment (Fu and Rich, 2002). The model creates upward looking

hemispherical viewsheds which are used to compute the solar insolation for each location and produce accurate insolation maps. The model uses a digital elevation model (DEM) as a major input and takes into account location latitude and altitude, surface slope and aspect; shadows cast surrounding topography, daily and seasonal shifts in solar angle, and atmospheric attenuation.

The main objective of the Flint Geothermal Project has been to integrate remote sensing data with geological data such as faults, geochemistry and geothermometry to identify and delineate areas of geothermal activity in Colorado. The specific objectives of the project are to:

1. Search, obtain and review remote sensing data from different sensors onboard different satellites such as ASTER, Thematic Mapper (TM) and/or Enhanced Thematic Mapper (ETM+).
2. Obtain GIS data such as transmission network, land ownership of Colorado, digital elevation model (DEM) of Colorado, Cities, Boundaries, etc.
3. Preprocess and analyze the data for identifying thermal signatures.
4. Produce a map or maps showing the thermally active areas, i.e. areas have anomalous surface temperature.
5. Provide conclusions and recommendations from the study on the best targets for further investigation.

2. Study Area and Data

The study area covers the western slope of the State of Colorado (Figure 1). Initially, the project was designed to cover the entire State, however, the area is too large for the purposes of the current research scope. It has not thought to be feasible to try to effectively analyze data for the entire State given the Project's schedule and budget. Moreover, the geology of the eastern slope is covered under thick alluvial deposits which obscure features associated with geothermal activities. Targets of interest within the study area were those which have anomalous surface temperatures and may also have some geothermal features, such as hot springs, associated with them.

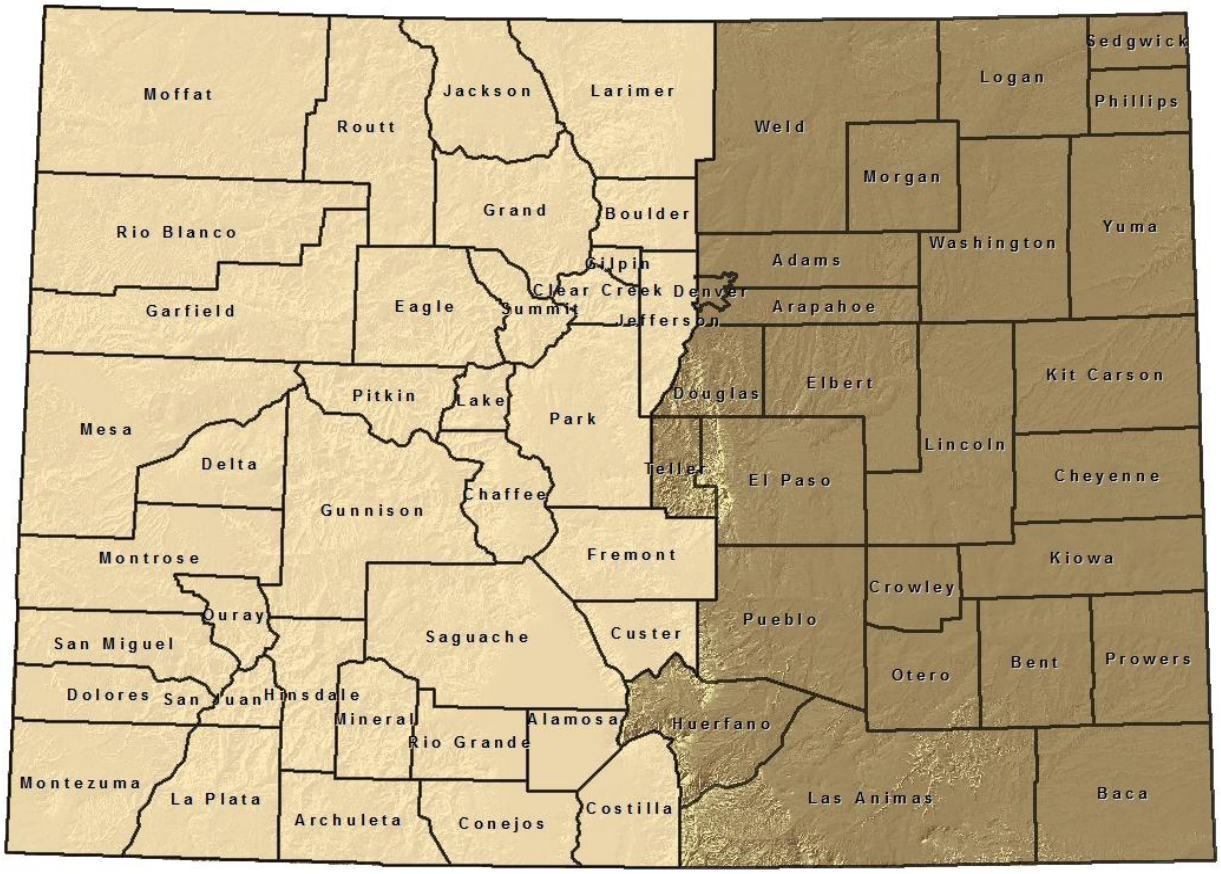

Figure 1. Shaded relief map of Colorado State showing the study area (beige shade).

Remote sensing data from sensors onboard NASA's Lansat and Terra platforms were obtained. Data from Thematic Mapper (TM) and Enhanced Thematic Mapper Plus (ETM+) onboard Landsat platforms and Advanced Spaceborne Thermal Emission and Reflection Radiometer (ASTER) aboard the Terra satellite were downloaded from Earth Resources Observation Systems (EROS) Data Center. 12 Landsat scenes that cover western Colorado, in total 24 Landsat scenes, i.e. a pair of scenes acquired on different dates, and 94 ASTER scenes acquired in the period between 2000 and 2007 were obtained. Also other datasets were obtained from United Sates Geological Survey (USGS), Colorado Geological Survey (CGS), and other data sources. The data include: 30-m digital elevation model, NLCD 2001 land cover classification raster data (land cover and land use types), Colorado deep-seated faulting (mapped shear zones, regional and young faults), isostatic gravity, transmission network and substations, land ownership (Bureau of Indian Affairs, Bureau of Land Management, Bureau of Reclamation, Department of Defense, Local Government, National Park Service, Private, State, United States

Forest Service, and United States Fish and Wildlife Service), bottom-hole temperatures from oil and gas well database, geologic maps and rock units, Colorado mineral belt, State of Colorado geographic information (borders, cities, roads, highways, etc.), Colorado thermal wells/springs and heat flow data points, geochemistry, and geothermometry.

3. Approach and Methodology

To achieve our objective of identifying geothermally active areas in Colorado a hierarchical approach was adopted in which we examined data from Thematic Mapper (TM), Enhanced Thematic Mapper Plus (ETM+) and Advanced Spaceborne Thermal Emission and Reflection Radiometer (ASTER) to digitally model hot/warm surface exposures. Geological characteristics such as faulting and other available datasets of known geothermal features in Colorado were used. Candidate areas were identified with TM, ETM+, and ASTER data and ranked for commercial geothermal potential.

3.1. Retrieval of Land Surface Temperature

3.1.1 Landsat Land Surface Temperature

Land surface of Colorado is heterogeneous with many different land use and land cover types. As a result the surface throughout the State has variable emissivities. Therefore, temperatures of different land use and land cover types were calculated. Landsat data were analyzed for 9 Colorado's land cover types (open water, barren, deciduous forest and evergreen forest, mixed forest, shrub/scrub, grassland/herbaceous, pasture hay, and cultivated crops). The digital numbers of each Landsat scene were converted to radiance using **Equation 1**. The temperature of each pixel within each scene was calculated using the thermal band. An average emissivity value was used for each land cover type within each scene. The temperature was calculated in degrees Kelvin by **Equation 3** and then converted to degrees Celsius for each land cover type. This process was repeated for each of the land cover types. The vector file of each land cover type was used to mask the temperatures of the pixels which were covered by this cover type. The NLCD 2001 land cover classification raster data of the zones that cover Colorado was used to identify the land cover types within each scene.

$$P_R = G(P_{DN}) + B \quad (1)$$

where:
P_R = Pixel radiance value
P_{DN} = Pixel digital number
B = Bias (offset)
G = Gain (calculated using equation 2)

$$Gain = \frac{(LMAX - LMIN)}{(\mathrm{QCALMAX} - \mathrm{QCALMIN})} \quad (2)$$

where:
LMAX = the spectral radiance that is scaled to QCALMAX in W/(m^2 sr μm)

LMIN = the spectral radiance that is scaled to QCALMIN in W/(m^2 sr μm)
QCALMAX = the maximum quantized calibrated pixel value (corresponding to $LMAX_\lambda$) in DN

QCALMIN = the minimum quantized calibrated pixel value (corresponding to LMIN) in DN

$$T_K = \frac{K_2}{\ln[\frac{K_1}{P_R} + 1]} \quad (3)$$

where:
T_K = Temperature in degrees Kelvin
P_R = Pixel radiance value
K_1 = 607.76 (Landsat TM)
K_2 = 1260.56 (Landsat TM)
K1 = 666.09 (Landsat ETM+)
K_2 = 1282.71 (Landsat ETM^+)

Note: K_1 and K_2 for TM. ETM^+ has different values

3.1.2. ASTER Land Surface Temperature

Land surface of Colorado, as mentioned earlier, is heterogeneous composed of different land use and land cover types and in turn has variable emissivities. Therefore, the Emissivity Normalization Algorithm that separate temperature from emissivity has been employed to calculate the temperature of each pixel. The following steps were used for calculating the temperature: (1) an emissivity of 0.96 is used to calculate the temperature of each pixel from the 5 ASTER thermal channels (i.e. each pixel has 5 temperatures) using equation 4 (Kealy and Hook, 1993); (2) the highest temperature of step 1 is assigned as the temperature of the pixel and

used to calculate the emissivity of the surface of each channel; (3) calculated emissivity is then used to calculate the surface temperature.

$$T_i = \frac{C_2}{\lambda_i \, ln\left(\frac{\varepsilon C_1}{M_i \lambda_i^5 \pi} + 1\right)} \quad (4)$$

where:
T_i = temperature of channel i (K)
λ_i = wavelength of channel i (m)
Mi = blackbody radiance (W/m^2)
$\boldsymbol{\varepsilon}$ = emissivity
C_1 = first radiation constant (3.74151×10^{-16} W/m^2)
C_2 = second radiation constant ($0.0143879 \times 10^{-16}$ mK)

3.2. Retrieval of Insolation

The Solar Analyst model developed by Fu and Rich (1999) is used to calculate the incoming solar radiation for the each of the areas investigated. The model was developed to calculate the insolation for the day or part of the day during which the ASTER scenes were acquired. The model creates an upward looking hemispherical viewshed (the angular distribution of sky obstruction) for every location on the DEM. The hemispherical viewsheds are then used to calculate the insolation for each location and to produce an insolation map. The model calculated a viewshed by searching in a specified set of directions around a location of interest determining the maximum angle of obstruction (horizon angle) in each direction. Then the horizon angles were converted into a hemispherical coordinate system. The viewshed grid cell was identified with visible or obstructed sky directions. The grid cell location (row and column) corresponds to zenith and azimuth angles. The model divided the whole sky into a series of sky sectors defined by zenith and azimuth angles. Homogenous transmissivity and diffuse proportion parameters were used, because the ASTER scenes were practically free of clouds. The total solar radiation is composed of three components: direct, diffuse, and reflected. Hence, the reflected radiation from surroundings generally accounts for a small portion of the global radiation; the model then computes the direct and diffuse components (Fu and Rich 1999).

The direct solar radiation is calculated as a function of sun position at interval of half an hour throughout the day. The position of the sun is calculated based on latitude, day of the year and time of the day during which the scenes were acquired. The model also takes into account the penumbral effects. The total direct radiation for a ground location is computed as the sum of

direct radiation from all sky directions. The direct radiation of sky direction with a zenith angle θ and azimuth angle α is calculated using the following **Equation**:

$$DirIns_{\theta,\alpha} = S_{const} * \tau^{m(\theta)} * SunDur_{\theta,\alpha} * SunGap_{\theta,\alpha} * cos(AngIn_{\theta,\alpha}) \quad (5)$$

where:
S_{const} = the solar constant (1367 Wm^{-2})
τ = average transmittivity of the atmosphere
m = relative optical path length
$SunDur_{\theta,\alpha}$ = time duration represented by sky sector
$SunGap_{\theta,\alpha}$ = gap fraction (proportion of unobstructed sky area in each sky sector)
$AngIn_{\theta,\alpha}$ = angle of incidence between the centroid of the sky sector and the axis normal to the surface

The relative path (m) and $AngIn_{\theta,\alpha}$ are calculated with **Equations 6** and **7**, respectively.

$$m = exp(-0.000118 * elev - 1.638 * 10^{-9} * elev^2)/\cos(\theta) \quad (6)$$

$$AngIn_{\theta,\alpha} = \text{acos}[\cos(\theta) * \cos(G_z) + \sin(\theta) * \sin(G_z) * \cos(\alpha - G_a)] \quad (7)$$

where:
θ = solar zenith angle
$elev$ = elevation
G_z = surface zenith angle
G_a = surface azimuth angle

The Solar Analyst calculates the incoming diffuse radiation as uniform, i.e. the same from all sky directions, or the diffuse radiation varies with zenith angle. This study assumed that diffuse radiation flux was uniform over the area covered by ASTER scene. The diffuse radiation is integrated over half an hour interval and corrected by the gap fraction and angle of incidence using **Equation 8**.

$$DiffIns_{\theta,\alpha} = R_{glob} * P_{diff} * Dur * SkyGap_{\theta,\alpha} * Weight_{\theta,\alpha} * cos(AngIn_{\theta,\alpha}) \quad (8)$$

where:
R_{glob} = global normal radiation (calculated using equation 5)
P_{diff} = diffuse proportion of global normal radiation flux
Dur = time interval
$SkyGap_{\theta,\alpha}$ = gap fraction (proportion of visible sky) for the sky sector

$Weight_{\theta,\alpha}$ = proportion of diffuse radiation originating in a given sky sector relative to all sectors (calculated using equation 6)
$AngIn_{\theta,\alpha}$ = angle of incidence between the centroid of the sky sector and the axis normal to the surface

Global normal radiation (R_{glob}) is calculated by summing up the direct radiation from every sky sector including the obstructed ones without correcting for angle of incidence and then correcting for proportion of direct radiation (**Equation 9**).

$$R_{glob} = \left(S_{const} \sum \tau^{m(\theta)}\right)/\left(1 - P_{diff}\right) \quad (9)$$

$Weight_{\theta,\alpha}$ for uniform diffuse radiation is calculated using the following equation:

$$\mathrm{Weight}_{\theta,\alpha} = (\cos\theta_2 - \cos\theta_1)/\mathrm{Div}_{\mathrm{azi}} \quad (10)$$

where:
θ_1, θ_2 = zenith angles bounding the sky sector
Div_{azi} = number of azimuthal division in the sky map

Total diffuse radiation is computed as the sum of the diffuse solar radiation ($DiffIns_{\theta,\alpha}$) and the global solar radiation is calculated as the sum of direct and diffuse radiation of all sectors.

3.3. Identification of Thermal Anomalies

Calculated temperatures were used to statistically identify and delineate the geothermal areas. Figure 2 shows, as an example, the temperature distribution of one ASTER nighttime scenes. The mean temperature and the standard deviation (σ) of the temperature residuals of each scene were calculated and used to identify areas that had temperatures, equal to, mean plus 1σ, mean plus 2σ, and greater than mean plus 2σ. Areas that had temperature residuals greater than 2σ, and areas with temperature equal to 1σ to 2σ, were considered ASTER modeled very warm and warm surface exposures (thermal anomalies), respectively.

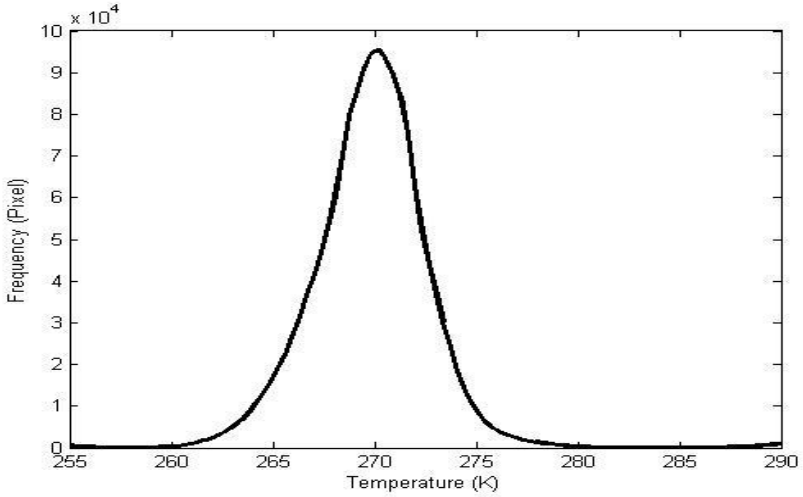

Figure 2. Temperature distribution of one ASTER nighttime scene.

3.4. Selection of Potential Geothermal Active Areas

The geologic data was integrated with remote sensing data in ArcGIS. A ranking system was developed for selecting areas of high potential geothermal signature. The ranking system was created based on the hot/warm surface exposures identified from remote sensing data and geological characteristics. The geological characteristics are important in selection of the potential targets, because they minimized the risk of selecting false thermal anomalies identified by remote sensing data. The criteria used for the ranking system included: hot/warm surface exposures modeled from ASTER/Landsat satellite imagery, alteration mineral commonly associated with hot springs (clays, Si, and FeOx) modeled from ASTER and Landsat data, the Colorado Geological Survey (CGS) known thermal hot springs/wells and heat-flow data points, Colorado deep-seated fault zones, weakened basement identified from isostatic gravity data, and Colorado sedimentary and topographic characteristics. Each of these criteria were assigned points with total points adding to eleven (i.e. a perfect target will score was eleven points).

4. Target Areas

The use of remote sensing thermal data in integration with geologic, geochemistry, and geothermometry data can be used to identify areas of geothermal activities; however, sometimes it is difficult to distinguish between the geothermal anomalies and others caused by sources originating from the interaction between incoming solar radiation and surface orientation (slope

and aspect). Employment of solar radiation model with analyzed thermal infrared (TIR) data has improved the possibility of correctly identifying geothermally active areas due to the fact that the solar and topographic effects have been eliminated or significantly reduced.

4.1. Potential Target Areas

Based on the ranking system 29 potential target areas were selected (Figure 3). The top Six (6) were initially selected. As field work progressed and after obtaining geochemistry and geothermometry data 8 more targets were added for field visits. Some of the selected areas were visited and temperature measurements were taken using 2-meter temperature surveys. The data obtained from the field were analyzed and evaluated. The results of the analysis revealed that some of the areas were falsely identified as geothermal active areas by remote sensing. This was mainly due to solar and topographic effects. As a result the methodology needed to be revised and modified so as to eliminate or minimize the false positives. A spatial based insolation model that took into consideration the surface orientation was employed to calculate the incoming solar radiation. The results were then used to compute the contribution of solar radiation in surface temperature. This was accomplished by converting the insolation to temperature using emissivity values calculated from ASTER data.

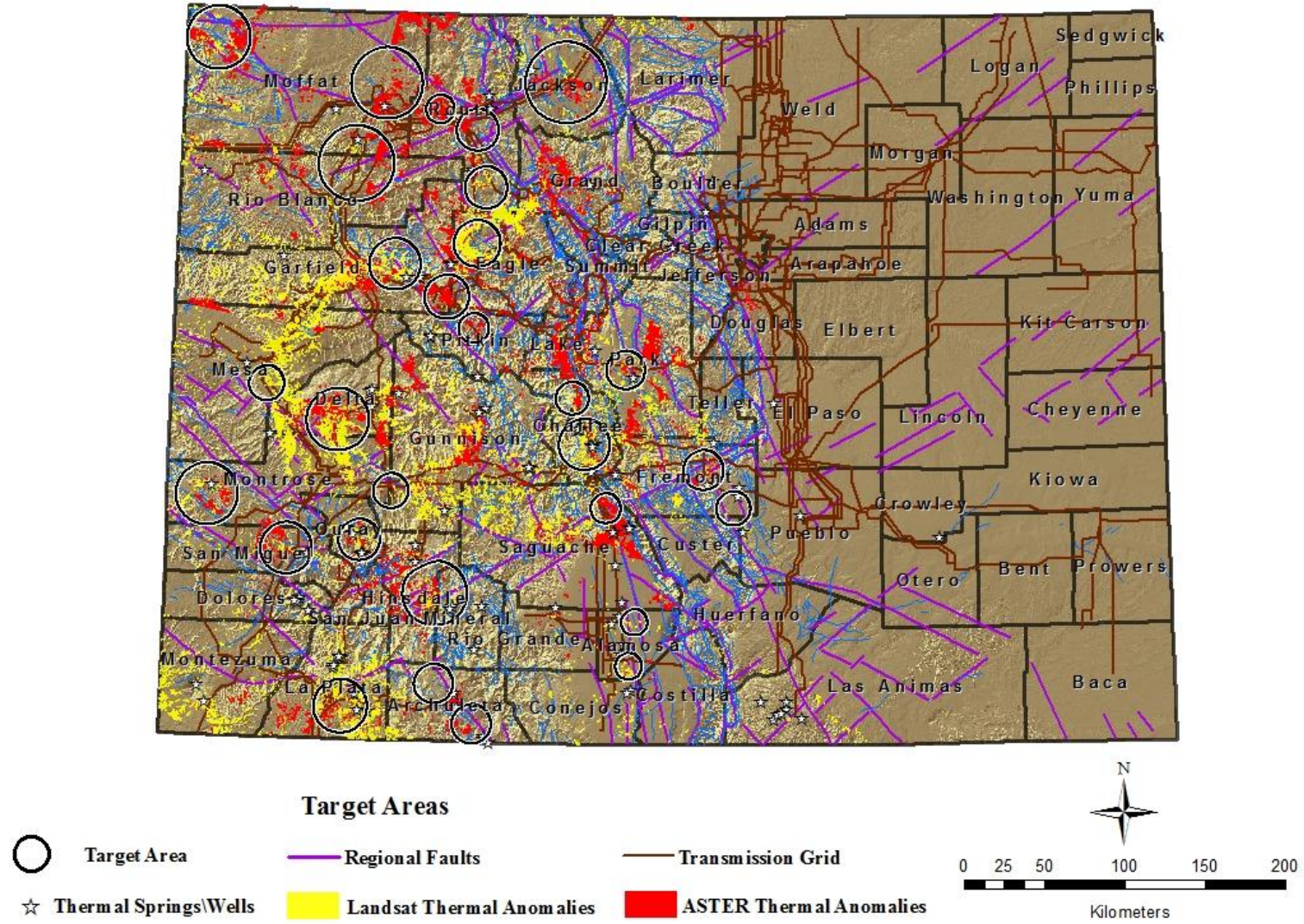

Figure 3. Potential target areas (black circles).

4.2. Combining Spatial-based Insolation Model and ASTER Thermal Data

4.2.1. Insolation Map

The Solar Analyst model was used to calculate the insolation of the selected potential target areas. As an example, the global insolation (direct and diffuse radiation) map on the day the ASTER nighttime data was acquired over Chaffee County is shown in Figure 4. Topography, surface slope, aspect and shadows created by topographic features were the main factors causing a modification of the distribution of incoming solar radiation. These led to high spatial variations in the amount of insolation received by the surface. This in turn resulted in variability of surface temperature. The warm colors indicate areas that received high amount of solar radiation. These were on areas of gentle slope and/or not obscured by topography and facing south. Lower insolation values depicted by cool colors were mostly on the north facing slopes and on areas where the sky is blocked by topography.

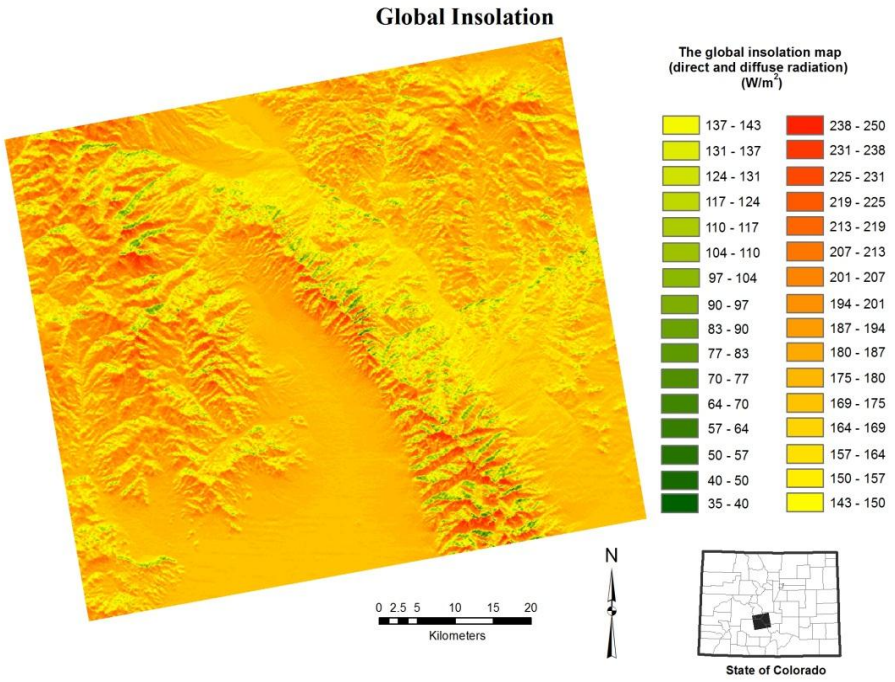

Figure 4. Map of the global insolation received by the surface during the day ASTER nighttime image was acquired over Chaffee County.

4.2.2. Temperature

The results revealed that some areas in the study area had high temperatures. This was mainly due to a major contribution of incoming solar radiation, directed by surface orientation as well as topographic characteristics. For example, see the areas outlined by boxes in Figure 5a. It was difficult to distinguish between high temperatures due to geothermal activities and others caused by solar radiation and surface orientation effects. These topographic and surface orientation effects needed to be corrected. Under the assumption that the land surface temperature due to solar radiation is mostly generated by the insolation received by the surface during the day ASTER scene was acquired, the modeled insolation was converted to temperature using the emissivities calculated from ASTER data. If the area beneath the surface had a geothermal signature then the residual of temperatures was calculated from ASTER thermal data. The modeled insolation was then composed mostly temperature due to geothermal heat (Figure 5b). Incorporating this insolation model that calculates the spatial variations in the coming solar radiation with ASTER temperature significantly reduced the false positives caused by the effects of solar geometry and topography.

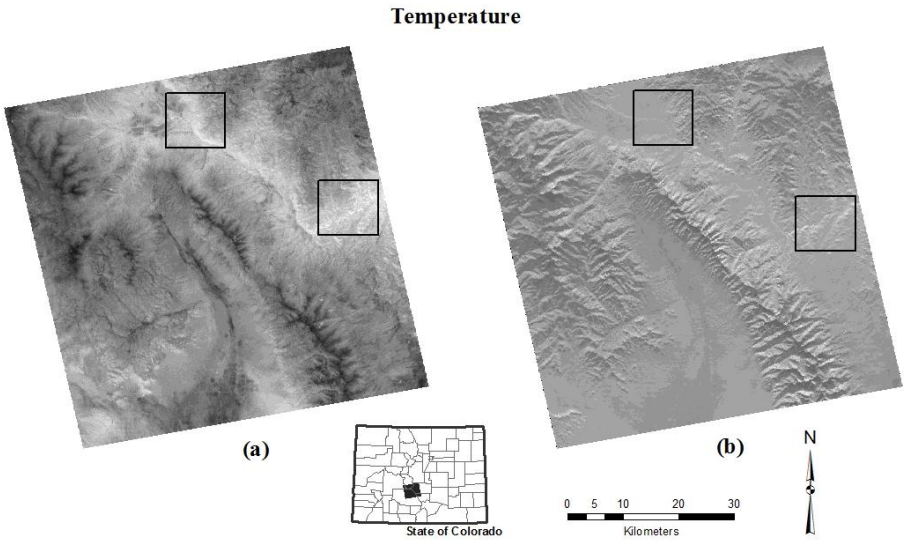

Figure 5. (a) Temperature calculated from ASTER thermal data, and (b) the residual temperature (insolation temperature subtracted from ASTER temperature). The boxes show some areas where the topographic and solar effects were eliminated or significantly reduced.

4.2.3. Selected Target Areas

The thermal anomalies obtained from the residual temperatures derived from remote sensing thermal data show that geothermal areas can be identified and delineated. From the potential areas, 6 target areas were recommended for further investigation during Phase II of the project. The areas were named after the county(s) within which the area is located. The areas are: Archuleta, Chaffee, Dolores, Garfield, Routt, and Saguache. Locations of the areas are shown in Figure 6-11.

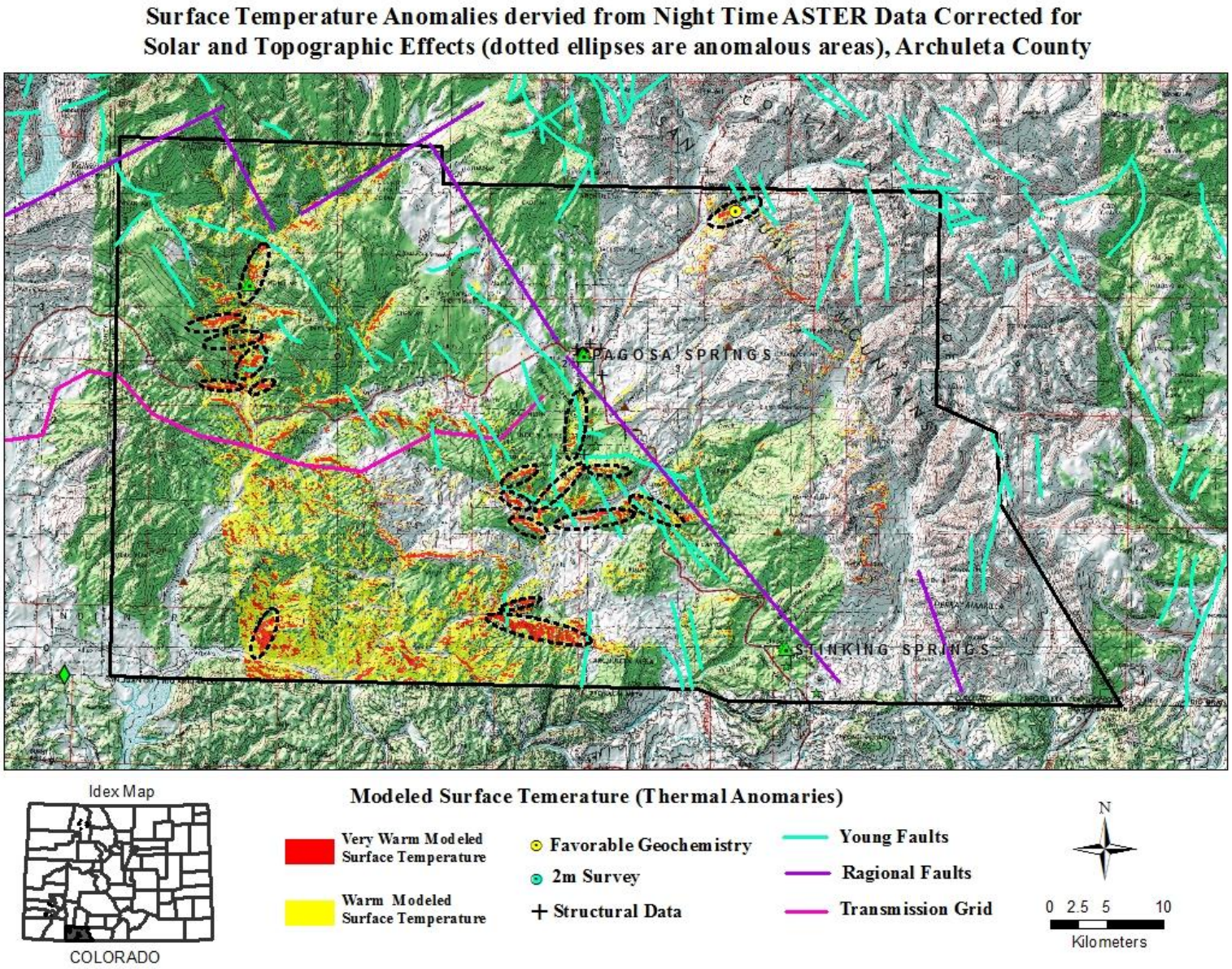

Figure 6. Location and features associated with geothermal activity of the Archuleta County target area.

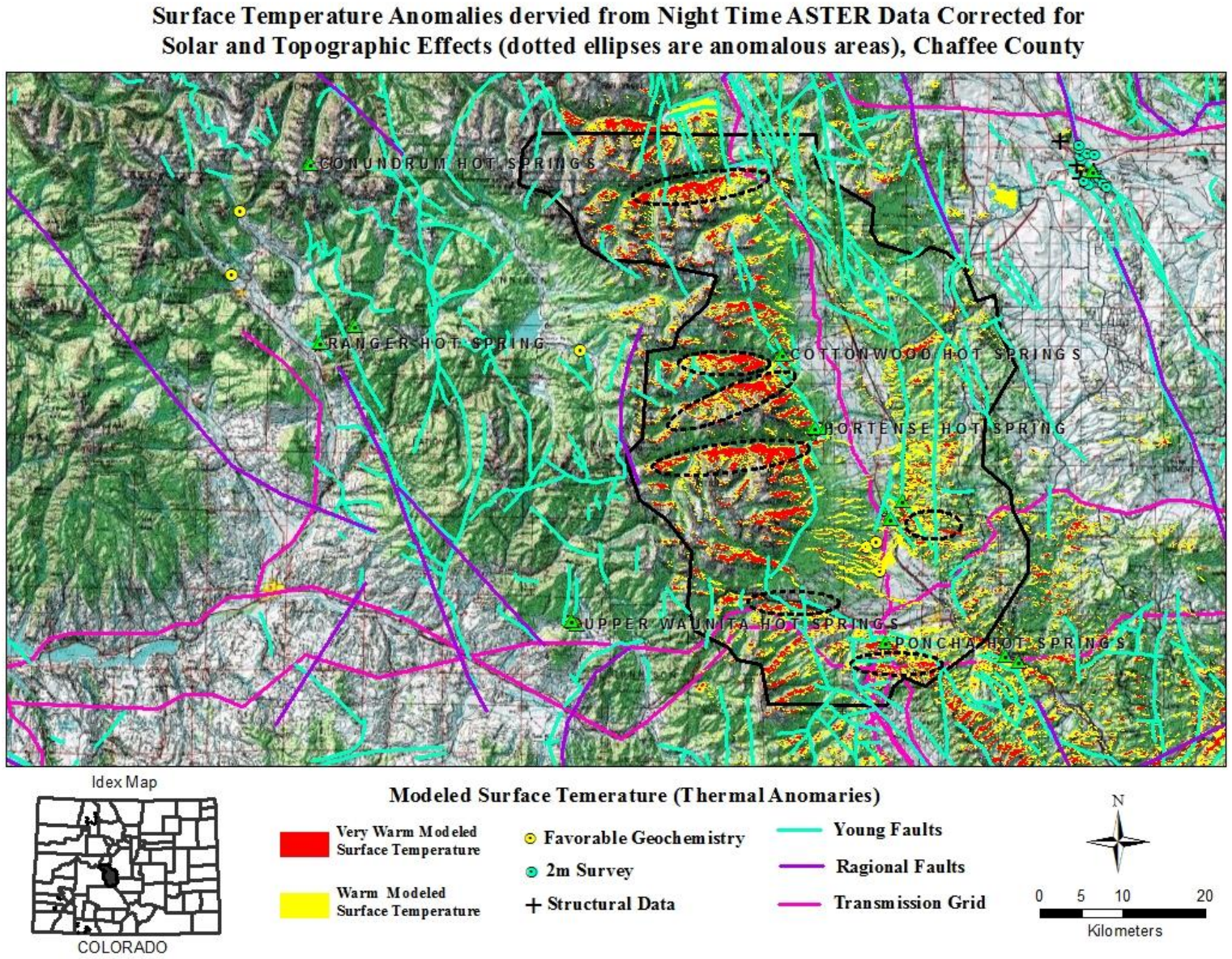

Figure 7. Location and features associated with geothermal activity of the Chaffee County target area.

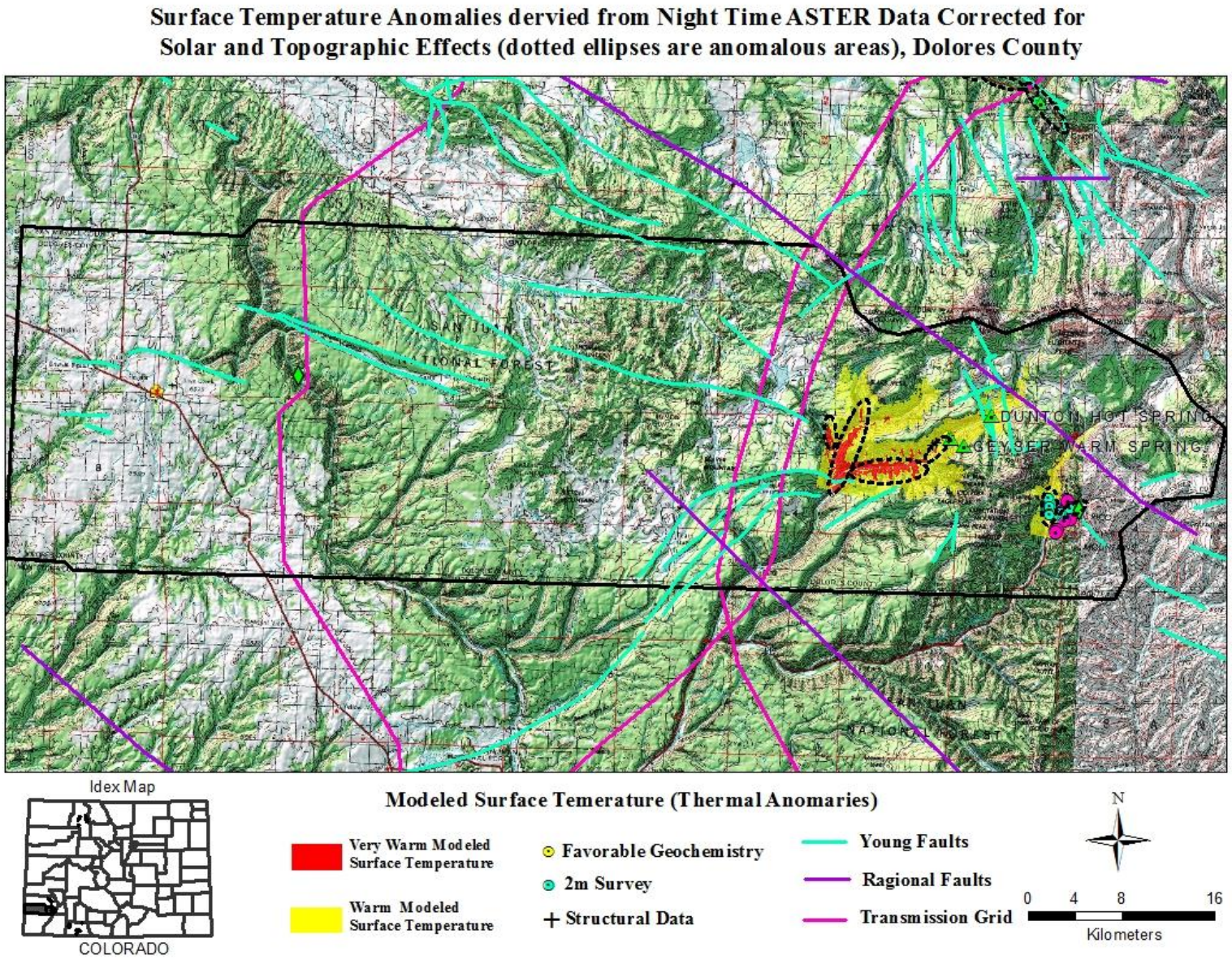

Figure 8. Location and features associated with geothermal activity of the Dolores County target area.

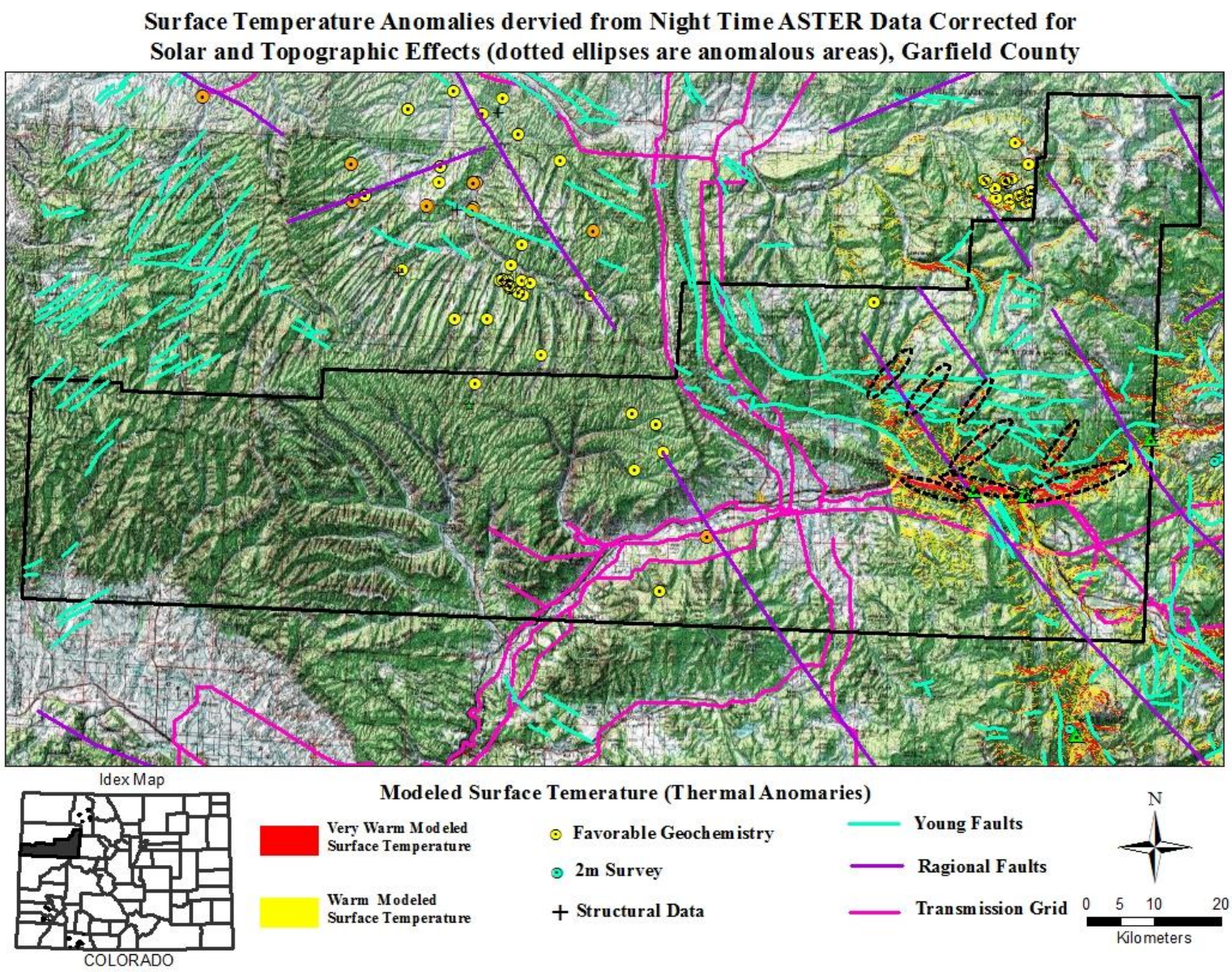

Figure 9. Location and features associated with geothermal activity of the Garfield target area.

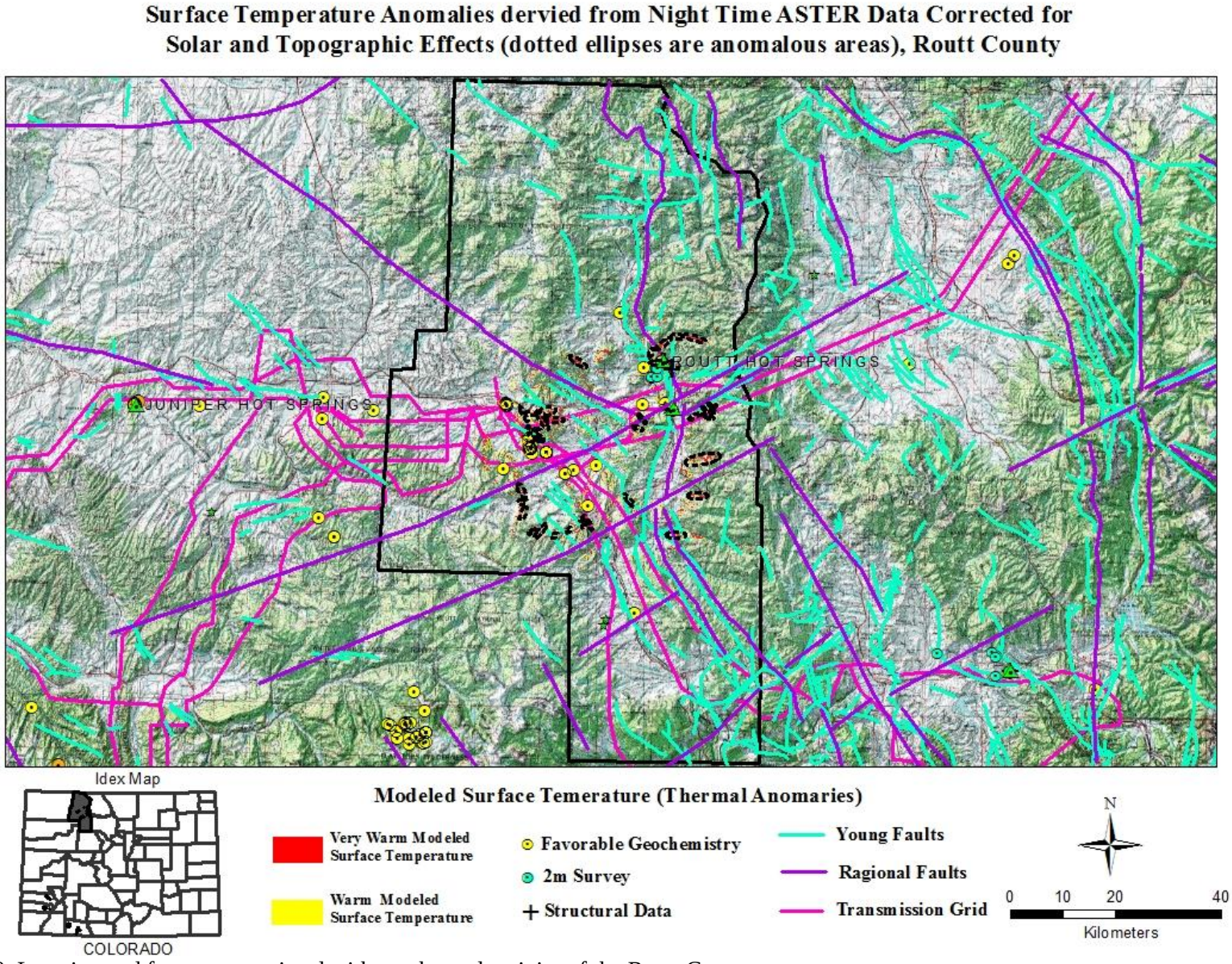

Figure 10. Location and features associated with geothermal activity of the Routt County target area.

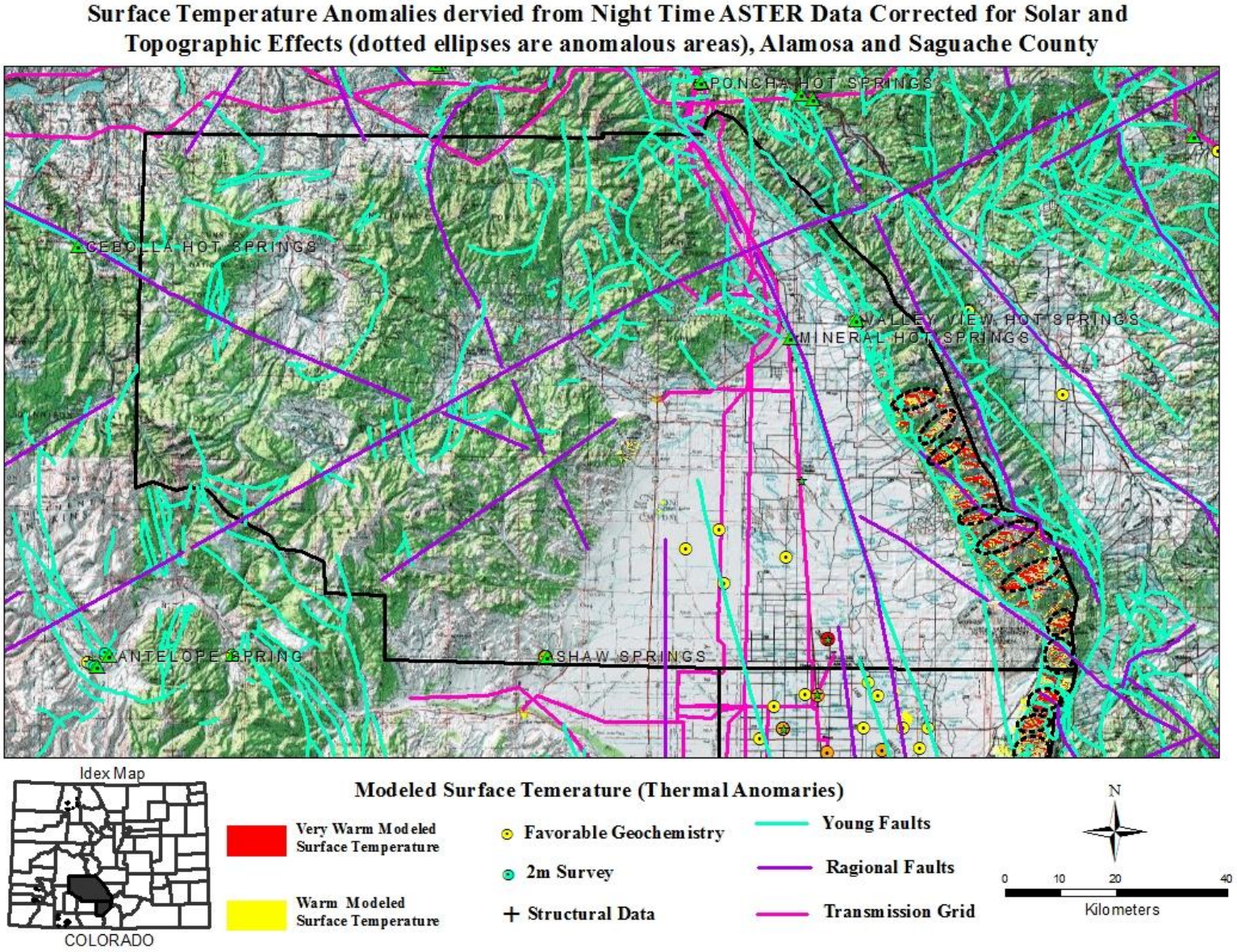

Figure 11. Location and features associated with geothermal activity of the Alamosa and Saguache Counties target area.

5. Discussion, Conclusions and Recommendations

The findings of the project indicate that thermal remote sensing can be used as a lead tool in detection and exploration of geothermal areas. However, two major difficulties limit the use of it; the first one is the accurate retrieval of land surface temperature (LST), and the second is the separation between LST due to incoming solar radiation and topographic effects and LST as a result of geothermal heat. Remotely sensed data is mainly affected by atmosphere, emissivity, and topography. Wan and Dozier (1989) found out that errors due to emissivity were greater than errors caused by atmospheric interactions.

The radiance emitted from the surface of the Earth in the thermal infrared region of electromagnetic spectrum depends on the temperature and the emissivity of the surface. The land surface of Colorado has variable chemistry and texture. Since the ground is composed of various land use and land cover types, the emissivity is variable. The calculation of temperature using Landsat thermal data was limited since Landsat's sensors have only one thermal band. Using average emissivity may result in errors of temperature values. This is compounded by the fact that emissivity values are not homogeneous over all land use or land cover types. However, Landsat is still valuable to explore large areas which need to be investigated.

Land surface temperatures of the study areas were recovered accurately using the 5 ASTER thermal bands. This was accomplished by employing temperature emissivity separation algorithm. This is a useful algorithm for recovering land surface temperature and emissivity from multispectral TIR remote sensing data (Gillespie et al., 1998). The Solar Analyst took into consideration the topographic, atmospheric, and surface orientation effects, thus it enabled the calculation of the incoming solar radiation with its spatial variations. The main advantage of the model is its ability to create maps of global radiation integrated over any period of time using the digital elevation model as an input with other few parameters.

The temperature due to geothermal heat is calculated as the residual of the ASTER temperature and the temperature due to incoming solar radiation. This technique eliminates or significantly reduces the solar and topographic effects and has advantages over the technique developed by Coolbaugh et al. (2007): (1) it can be applied to large areas using ASTER data given a digital elevation model available for any given area. This avoids the need for a pair of day- and nighttime data to apply the methodology. (2) No field data is required to correct for the

albedo and topography. (3) No geothermal features (e.g. hot springs) are priori needed to apply the technique, i.e. the technique is very useful in blind geothermal areas.

The analysis revealed that integrating ASTER thermal data with spatial-based insolation model eliminated or reduced the solar and topographic effects. This in turn improved the capability of identifying areas of geothermal activity using thermal remote sensing night- and daytime data.

Some areas have falsely been identified as geothermally active using temperature derived from the ASTER thermal data. This was mainly due to the topographic and surface orientation effects on the incoming solar radiation. There were obviously overestimations in regions that have received greater insolation than other areas. In contrast, there were some underestimated parts caused by the statistics biased towards areas that have high temperature due to solar and topographic effects. However, combining ASTER thermal data with the spatial based insolation model has significantly reduced the effects of spatial variation of insolation to identify geothermally active areas.

The following conclusions and recommendations can be drawn from the results of the study:

- Satellite remote sensing is very useful in detecting and identifying areas of geothermal activity. Thus remote sensing techniques can be used as a lead tool for the exploration of geothermal areas that have a high potential to serve as a geothermal energy source.
- Spatial insolation models are good tools for estimating the amount of incoming solar radiation received on surfaces of various topography and surface orientations.
- This technique is possibly one of the first attempts to develop an algorithm which uses remote sensing information and a spatial-based insolation model to locate areas of geothermal activity.
- ASTER thermal data can be used by integrating spatial-based insolation model results with remote sensing techniques to identify geothermal active areas.
- 6 areas were recommended for further field investigation during Phase II of the project which should be done properly and thoroughly. Given the fact that remote sensing data may contain georeferencing errors, designing field measurements should take that into consideration.

6. References

Anding, D., & Kauth, R. (1970). Estimation of sea surface temperature from space. Remote Sensing of Environment, 1, 217-220.

Barton, I. J. (1985). Transmission model and ground-truth investigation of satellite derived sea surface temperatures. Climate and Applied Metrology, 24, 508-516.

Coolbuagh, M. F., Kratt, C., Fallacaro, A., Calvin, W. M., & Taranik, J. V. (2007). Detection of geothermal anomalies using Advanced Spaceborne Thermal emission and Reflection Radiometer (ASTER) thermal infrared images at Brady's Hot Springs, Nevada, USA. Remote Sensing of Environment, 106, 350-359.

Eneva, M., Coolbaugh, M., Bjornstad, S., & Combs, J. (2007). Detection of surface temperature anomalies in the Coso Geothermal Field using thermal infrared remote sensing. GRC Transaction, 31, 335-340.

Eneva, M., Coolbaugh, M., & Combs, J. (2006). Application of satellite thermal infrared imagery to geothermal exploration in east central California. GRC Transaction 30, 407-411.

Eneva, M., & Coolbaugh, M. (2009). Importance of elevation and temperature inversions for the interpretation of thermal infrared satellite images used in geothermal exploration. GRC Transaction, 33, 467-470.

Fu, P., & Rich, M. P. (1999). Design and implementation of the Solar Analyst: an ArcView extension for modeling solar radiation at landscape scales. Proceedings of the Nineteenth Annual ESRI User Conference.

Fu, P., & Rich, M. P. (2002). "A Geometric Solar Radiation Model with Applications in Agriculture and Forestry." Computers and Electronics in Agriculture 37:25–35.

Gillespie, A., Rokugawa, S., Matsunaga, T., Cothern, S. J., Hook, S., & Kahle, B. A. (1998). A temperature and emissivity separation algorithm for Advanced Spaceborne Thermal Emission and Reflection Radiometer (ASTER) images. IEEE Transactions on Geoscience, 30(4), 1113-1126.

Green, B. D., & Nix, R. G. (2006). Geothermal-The Energy Under Our Feet: Geothermal Resource Estimates for the United States. Technical Report, NREL/TP-840-40665, November 2006.

Hook, J. S., Gabell, R. A, Green, A. A., & Kealy, S. P. (1992). A comparison of techniques for extracting emissivity information from thermal infrared data for geologic studies. Remote Sensing of Environment, 42, 123-135.

Kealy, S. P., & Hook, J. S. (1993). Separating temperature and emissivity in thermal infrared multispectral scanner data: Implications for recovering land surface temperatures. IEEE Transactions on Geoscience and Remote Sensing, 31(6), 1155-1164.

Kilpatrick, A. K., Podestfi, P. G., & Evans, R. (2001). Overview of the NOAA/NASA advanced very high resolution radiometer Pathfinder algorithm for sea surface temperature and associated matchup database. Geophysical Research, 106(C5), 9179-9197.

McConaghy, C. D. (1980). Measuring sea surface temperature from satellites. Remote Sensing of Environment, 10, 307-310.

McMillin, M. L., & Crosby, S. D. (1984). Theory and validation of the multiple window sea surface temperature technique. Geophysical Research, 89(C3), 3655-3661.

Noble, E. V. & Wilkerson, C. J. (1970). Sea surface temperature mapping flights-Norwegian Sea, summer 1968. Remote Sensing of Environment, 1, 187-193.

Prabhakara, C., Dalu, G., Kunde, G. V. (1974). Estimation of sea surface temperature from remote sensing in the 11- to 13-3μm window region. Geophysical Research 79(33), 5039-5044.

Spatial Analysis Center, Yellowstone National Park (Unpublished Material). Hydrogeothermal Areas of Yellowstone National Park, Wyoming, Montana, Idaho. Online_Linkage: \\inpyellgis2\data\yell_data\geothermal\y_thermareas.

Tang, S., Zhu, Q., Bai, X., Yang, S., Shuai, Y, & Bu, Q. (2004). A TES algorithm based on corrected Alpha difference Spectra. IEEE, 450-4503.

Tang, S., Li, X., Wang, J., Zhu, Q., & Zhang, L. (2007). An improved TES based on the corrected ALPHA difference spectrum. Science in China Series D-Earth Sciences, 50(2), 274-282.

Vaughan, R. G., Keszthelyi, L. P., Lowenstern, J. B., Jaworowski, C., & Heasler, H. (2012). Use of ASTER and MODIS thermal infrared data to quantify heat flow and hydrothermal change at Yellowstone National Park. Journal of Volcanology and Geothermal Research, 233-234, 72-79.

Walton, C. (1985). Satellite measurement of sea surface temperature in the presence of volcanic aerosols. Climate and Applied Meteorology, 24(6), 501-507.

Wan, Z., & Dozier, j. (1989). Land-surface temperature measurement from space: physical principles and inverse modeling. IEEE Transactions on Geoscience and Remote Sensing, 27(3), 268-278.

Wood, C. A., & Kienle, J. (1990), Volcanoes of North America: United States and Canada: Cambridge University Press, 354p, contribution by Christiansen, R. L.